

# Phase stability and pressure-induced structural transitions at zero temperature in $\text{ZnSiO}_3$ and $\text{Zn}_2\text{SiO}_4$

S.Zh. Karazhanov<sup>1-3\*</sup>, P. Ravindran<sup>1</sup>, P. Vajeeston<sup>1</sup>, A.G. Ulyashin<sup>2†</sup>, H. Fjellvåg<sup>1</sup>, and B.G. Svensson<sup>4</sup>

<sup>1</sup> Centre for Material Science and Nanotechnology, Department of Chemistry, University of Oslo, PO Box 1033 Blindern, N-0315 Oslo, Norway

<sup>2</sup> Institute for Energy Technology, P.O.Box 40, NO-2027 Kjeller, Norway

<sup>3</sup> Physical-Technical Institute, 2B Mavlyanov St., Tashkent, 700084, Uzbekistan

<sup>4</sup> Department of Physics, University of Oslo, PO Box 1048 Blindern, N-0316, Oslo, Norway

## Abstract

Using density functional total energy calculations the structural phase stability and pressure-induced structural transition in different polymorphs of  $\text{ZnSiO}_3$  and  $\text{Zn}_2\text{SiO}_4$  have been studied. Among the considered monoclinic phase with space groups  $P2_1/c$  and  $C2/c$ , rhombohedral ( $R\bar{3}$ ), and orthorhombic ( $Pbca$ ) modifications the monoclinic phase ( $P2_1/c$ ) of  $\text{ZnSiO}_3$  is found to be the most stable one. At high pressure monoclinic  $\text{ZnSiO}_3$  ( $C2/c$ ) can coexist with orthorhombic ( $Pbca$ ) modification. Difference in equilibrium volume and total energy of these two polymorphs are very small, which indicates that it is relatively easier to transform between these two phases by temperature, pressure or chemical compositions. It can also explain the experimentally established result of metastability of the orthorhombic phase under all conditions. The following sequence of pressure induced structural phase transitions are found for  $\text{ZnSiO}_3$  polymorphs: monoclinic ( $P2_1/c$ )  $\rightarrow$  monoclinic ( $C2/c$ )  $\rightarrow$  rhombohedral ( $R\bar{3}$ ). Among the rhombohedral ( $R\bar{3}$ ), tetragonal ( $I\bar{4}2d$ ), orthorhombic ( $Pbca$ ), orthorhombic ( $Imma$ ), cubic ( $Fd\bar{3}m$ ), and orthorhombic ( $Pbnm$ ) modifications of  $\text{Zn}_2\text{SiO}_4$ , rhombohedral phase is found to be the ground state. For this chemical composition of the zinc silicate the following sequence of structural phase transitions is found: rhombohedral ( $R\bar{3}$ )  $\rightarrow$  tetragonal ( $I\bar{4}2d$ )  $\rightarrow$  orthorhombic ( $Pbca$ )  $\rightarrow$  orthorhombic ( $Imma$ )  $\rightarrow$  cubic ( $Fd\bar{3}m$ )  $\rightarrow$  orthorhombic ( $Pbnm$ ). Based on the analogy of crystal structures of magnesium and zinc silicates and using the lattice and positional parameters of  $\text{Mg}_2\text{SiO}_4$  as input, structural properties of spinel  $\text{Zn}_2\text{SiO}_4$  have also been studied.

**PACS:** 61.50.Ks; 81.30.Hd; 31.15.Ar

**Keywords:** Zinc silicates, phase transition, interface

\*Corresponding author: **E-mail:** smagul.karazhanov@ife.no

†Present address: SINTEF, Materials and Chemistry, P.O. Box 124 Blindern, NO-0314 Oslo, Norway

## 1. Introduction

Studies of the interface between semiconductors and transparent conducting oxides (TCO) present much interest for optoelectronic device technology. During fabrication of device structures based on contact semiconductor/TCO a mutual diffusion of the atoms from semiconductor to TCO and vice versa can take place at the interface. At high concentrations of the diffused atoms structural phase transformations can occur, which can result in formation of new compounds at the interface. Such compounds often possess wide band gap and form band offset with the semiconductor and TCO. From this point of view knowledge of structural properties, electronic structure, and optical properties of the compounds formed at the interface is important to use them in optoelectronic devices. Further, the crystal structure of compounds formed at the interface will be different from that of the bulk materials due to the interfacial effect and stress in the lattice. So, the structural phase stability studies on such compounds with pressure are both fundamental and technological significance. It can help to reveal how the interface influences operation of a particular device and to provide the information required to control the properties of the interface layer.

ZnO and Si are the compounds extensively used in modern semiconductor electronics. Electronegativity of Si and Zn are 1.90 and 1.65, respectively, which are close to each other. The atomic sizes of these elements are also comparable to each other i.e. 0.117 nm for Si and 0.133 nm for Zn. These data indicate that the diffusion of Si into ZnO can be favorable. As a result, at the interface in the heterostructures of Si/ZnO and SiO<sub>2</sub>/ZnO the Si and Zn related oxides can be formed, which will affect the device performance. Polymorphs of ZnSiO<sub>3</sub> and Zn<sub>2</sub>SiO<sub>4</sub> can be such interfacial oxide layers formed in between Si/ZnO and SiO<sub>2</sub>/ZnO[(1-2)] due to the solid state reaction. These compounds are of particular technological interest for thin film Si solar cells,[(3-6)] devices where ZnO deposited on silicate glass as a TCO buffer layer,[(7)] light-emitting diodes,[(8)] ZnO nanowires and nanotips grown on Si and Si on sapphire,[(9)] ZnO particles embedded in sol-gel silica,[(1)] nanostructures, etc..[(10-16)] The monoclinic ZnSiO<sub>3</sub> nanocrystals have been formed as a result of rapid thermal annealing of SiO<sub>2</sub> with metallic Zn nanocrystals.[(17)] Also by the transmission electron microscopy (TEM) with a focused electron beam irradiation process ZnSiO<sub>3</sub> nanoparticles have been found in a SiO<sub>2</sub> layer located in between the ZnO thin film and the Si substrate.[(18)] Moreover, from x-ray diffraction, TEM, and selected-area

electron diffraction studies it has been found that orthorhombic  $\text{ZnSiO}_3$  can be formed at the interface of the ZnO/Si heterostructure after annealing at 900 °C resulting from the inter-diffusion between ZnO and Si. [(19)]

Crystal structure and structural phase transitions of  $\text{ZnSiO}_3$  and  $\text{Zn}_2\text{SiO}_4$  have been studied experimentally in the past by many authors (see, e.g., Ref. [(20-25)]) at high temperatures in the range 700-1500 °C and pressures 0-17 GPa.  $\text{ZnSiO}_3$  in the monoclinic phase with space group (SG)  $C2/c$  is generally not found to be stable at atmospheric pressure and it can be obtained as a result of the reaction of willemite  $\text{Zn}_2\text{SiO}_4$  with quartz at about 3 GPa and subsequent transition to ilmenite at 10-12 GPa. [(20-25)] or 15 GPa. [(26)] However, it is reported in Ref. [(21)] that  $\text{ZnSiO}_3$  with SG  $C2/c$  exist at room temperature and ambient conditions also. Upon increasing the pressure, this phase can undergo the following sequence of displacive phase transitions from  $C2/c$  to a high pressure phase with SG  $P2_1/c (-m_1)$  at 1.92 GPa, which can also be transformed to another high pressure phase with SG  $C2/c (-m_2)$  at 4.9 GPa. However, the differences in equilibrium volumes between the latter three structural modifications of  $\text{ZnSiO}_3$  are too small to consider them as different polymorphs. Orthorhombic ( $-o$ ;  $Pbca$ )  $\text{ZnSiO}_3$  has been synthesized at high pressures and temperatures (see, e.g., Ref. [(24)]) and it is found to be metastable under all conditions.

In the polymorphs of  $\text{ZnSiO}_3$ , Zn atoms are coordinated both octahedrally and tetrahedrally [(24)] (Fig. 1). In  $\text{ZnSiO}_3\text{-}o$  the Zn atoms at the octahedral sites have irregular octahedral coordination to the O atoms.  $\text{ZnSiO}_3$  of trigonal/rhombohedral ( $-r$ ) symmetry with space group  $R\bar{3}$  is known by mineral name ilmenite.  $\text{ZnSiO}_3\text{-}r$  consists of a slightly distorted hexagonal close-packing array of O atoms with Zn and Si atoms in the interstices. Structural properties of these compounds have been analyzed more in detail in Refs. [(20, 23, 27)]. However, phase stability of different modifications of  $\text{ZnSiO}_3$  at low temperatures is not yet discussed in detail. According to Ref. [(26)] structural transition from  $\text{ZnSiO}_3\text{-}m_2$  to  $-r$  occurs at 15 GPa at 1000 °C.

The  $\text{Zn}_2\text{SiO}_4$  reported in Ref. [(28)] has been formed as a result of annealing the ZnO-SiO<sub>x</sub> system., Willemite  $\text{Zn}_2\text{SiO}_4$  has been formed as a result of the reaction of ZnO with SiO<sub>2</sub>, [(29)] which has lead to decrease of concentration of the O vacancies and Zn interstitials.  $\text{Zn}_2\text{SiO}_4$  has been used to synthesize the Si doped ZnO nanobelts. [(30)]

Phase transformations of  $\text{Zn}_2\text{SiO}_4$  have been studied[(31, 24, 27)] up to pressures  $\leq 17$  GPa and temperatures  $800\text{ }^\circ\text{C} - 1500\text{ }^\circ\text{C}$ . The following sequence of structural transformations have been found[(27)] between five polymorphs of  $\text{Zn}_2\text{SiO}_4$ : rhombohedral( $r$ )  $\rightarrow$  tetragonal( $t$ )  $\rightarrow$  monoclinic( $m$ )  $\rightarrow$  orthorhombic( $o_1$ )  $\rightarrow$  orthorhombic( $o_2$ )  $\rightarrow$  orthorhombic( $o_3$ ). Here the  $o_1$ ,  $o_2$ , and  $o_3$  modifications of the orthorhombic  $\text{Zn}_2\text{SiO}_4$  denote those with SG symmetry  $Pbca$ ,  $Imma$ , and  $Pbnm$ , respectively. Owing to the preference of Zn for tetrahedral rather than octahedral coordination by oxygen at low pressures, the  $\text{Zn}_2\text{SiO}_4$  crystallizes into the phenacite-structure with Zn atoms located in distorted octahedral coordination. [(14, 26, 22-23)] In  $\text{Zn}_2\text{SiO}_4$ - $t$  the oxygen atoms join together to Si and Zn so that each of the oxygen at the  $\text{SiO}_4$  tetrahedra is bonded to Zn atoms thus forming an integrated part of a Zn-O-Si network (see Fig. 2). The O atoms are located approximately in the body-centered cubic arrangement in  $\text{Zn}_2\text{SiO}_4$ - $t$ , while both the Zn and Si atoms are in tetrahedral coordination to the O atoms. In rhombohedral  $\text{Zn}_2\text{SiO}_4$  also the Zn and Si atoms are tetrahedrally coordinated to O atoms, where the Zn atoms occupy two crystallographically different sites, but the environments around these sites differ only slightly. Although there is no information about spinel structure of  $\text{Zn}_2\text{SiO}_4$ , similar type of compound  $\text{Mg}_2\text{SiO}_4$  posses it. The spinels are cubic ( $-c$ ). They are a class of minerals with the O ions forming a face-centered lattice where Zn cations are octahedrally coordinated and Si atoms are tetrahedrally coordinated.

The above mentioned experimental results about existence of different polymorphs of the zinc silicates, possibility of their formation at the interface between ZnO-Si and ZnO-SiO<sub>2</sub>, and possibility of phase transitions between the polymorphs creates the necessity to study structural properties, electronic structure, optical properties, as well as interface between the silicates and semiconductors. The study about electronic structure and optical properties of the intermixed zinc silicates has been performed in Ref. [(32)] which are found to be insensitive to crystal structure modifications and crystallographic directions. Still many questions have been left open. Some of them are the systematic study of band gap variation in between the zinc silicates and ZnO(Si) and the ways of controlling them, which would be important to know influence of the interface layer on current transport. The other one is doping of the silicates by shallow level impurities and H, which allows one to classify the silicates as semiconductors or insulators. However, first of all it is interesting to know which of the polymorphs of the zinc silicates is the most stable one, whether structural phase transitions can take place at low

temperatures and pressures as well and what is difference between equilibrium volumes of the polymorphs. In the present paper we intend to study these questions for  $\text{ZnSiO}_3$  *-o*, *-m<sub>1</sub>*, *-m<sub>2</sub>*, and *-r* as well as  $\text{Zn}_2\text{SiO}_4$  *-t*, *-r*, *-m*, *-o<sub>1</sub>*, *-o<sub>2</sub>*, *-o<sub>3</sub>*, *-c*.

## 2. Methods

The computations have been performed using the density-functional theory (DFT) within the local-density approximation (LDA). Structural relaxations and calculation of total energies have been performed with the projector-augmented-wave method (PAW) [(33-34)] as implemented in the Vienna *ab initio* simulation package (VASP)[(35)] using the Ceperley-Alder data[(36)] for the correlation energy in the parameterization by Perdew-Zunger.[(37)] The Zn-3*d*, and -4*s*, O -2*s* and -2*p*, Si-3*s* and -3*p* have been considered as the valence electrons. The self-consistent calculations were performed using a 4×4×4 mesh of special **k**-points. Test calculations showed that plane-wave cutoff energy of 500 eV is sufficient to describe structural properties of zinc silicates reliably. The convergence was achieved when the forces acting on the atoms were <10 meV Å<sup>-1</sup> and the total energy difference between two consecutive iterations were < 10<sup>-6</sup> eV.

The crystal structures are of different modifications of  $\text{ZnSiO}_3$  and  $\text{Zn}_2\text{SiO}_4$  are presented in Figs. 1 and 2, respectively. Experimentally determined lattice parameters and positional parameters[(38, 21)] have been used as input. All configurations were fully relaxed using the conjugate gradient method. Here it should be noted that there is some similarity between structural phase transitions and crystal structures of  $\text{ZnSiO}_3$  and  $\text{MgSiO}_3$ .[(20, 23-25)] The latter compound is well studied and is very important material to explore the mineralogy of the Earth's deep mantle. So,  $\text{MgSiO}_3$  can be used as a model system in the structural studies of  $\text{ZnSiO}_3$ . In the present paper this similarity shall be used. Due to lack of experimental data for positional and lattice parameters of  $\text{ZnSiO}_3$ -*r* and  $\text{Zn}_2\text{SiO}_4$ -*c* we have used those for  $\text{MgSiO}_3$ -*r* and  $\text{Mg}_2\text{SiO}_4$ -*c*, respectively as input for the structural optimization for these two phases.

## 3. Results

### 3.1 ZnSiO<sub>3</sub>

Structural optimization has been performed for all the considered structural modifications by the following procedure: first, atomic positions have been relaxed by force minimization method keeping the volume and shape of the crystal fixed. Using the relaxed atomic positions as input, the crystal volume and shape have been relaxed using stress minimization freezing out atomic positions. Then these optimized parameters have been used as input to relax atomic positions, cell volume and shape altogether. Crystal structure information obtained by this way was used as input for calculation of the total energy ( $E_{\text{tot}}$ ) as a function of the cell volume ( $V$ ). The minima ( $E_{\text{tot}}^{\text{min}}$ ) of the dependence  $E_{\text{tot}}(V)$  are taken as the equilibrium volume. Positional and lattice parameters derived from the DFT calculations for the equilibrium lattices are given in Table I together with experimentally determined values. Analysis of the Table I show that deviation of the calculated equilibrium volumes from the corresponding experimentally determined values by 2.3% for ZnSiO<sub>3-*o*</sub>, 3.3% for ZnSiO<sub>3-*m*<sub>1</sub></sub>, and 2.4% for ZnSiO<sub>3-*m*<sub>2</sub></sub>. The calculated positional parameters from the structural optimization are found to be overall in good agreement with experimental data. Symmetry of the optimized lattices were checked and found that it is the same as that of the experimentally determined one used as an input for the structural optimization.

Dependence of the total energy on volume has been analyzed for ZnSiO<sub>3</sub> (Fig. 3). The  $E_{\text{tot}}(V)$  for ZnSiO<sub>3-*o*</sub> is 2.3 meV higher in energy than ZnSiO<sub>3-*m*<sub>2</sub></sub> at their total energy minimum. Magnitude of the  $E_{\text{tot}}^{\text{min}}$  for ZnSiO<sub>3-*m*<sub>1</sub></sub> is found to be lower than that of ZnSiO<sub>3-*m*<sub>2</sub></sub> by about 10 meV. Consequently,  $m_2$  is the most stable phase.  $E_{\text{tot}}^{\text{min}}$  for ZnSiO<sub>3-*r*</sub> is found to be about 10 meV higher than that of ZnSiO<sub>3-*o*</sub> which indicates that ZnSiO<sub>3-*r*</sub> is the least stable among the considered phases. Since the difference in  $E_{\text{tot}}(V)$  between ZnSiO<sub>3-*o*</sub>, ZnSiO<sub>3-*m*<sub>1</sub></sub> and  $-m_2$  is not large, a small fluctuations of temperature and pressure can be sufficient to cause the phase transformation between these phases. This result could explain why metastability is observed experimentally for ZnSiO<sub>3-*o*</sub> at almost all conditions.[(24)]

Upon compression the volume dependence of  $E_{\text{tot}}$  for ZnSiO<sub>3-*m*<sub>1</sub></sub> intersects with that for  $-m_2$ ,  $-r$ , and  $-o$  (Fig. 3), which indicates the possibility of phase transition between these modifications. The present calculations suggest that upon compression the following sequence of structural phase transitions can take place: one from

ZnSiO<sub>3-*m*1</sub> to ZnSiO<sub>3-*m*2</sub> and the other from ZnSiO<sub>3-*m*2</sub> to ZnSiO<sub>3-*r*</sub> at pressures 6.8 and 8.5 GPa, respectively, with corresponding volume shrinkage at the phase transition point 1.1 and 5.24 Å<sup>3</sup> per formula unit. The calculated transition pressure of 6.8 GPa for the transition ZnSiO<sub>3-*m*1</sub> → ZnSiO<sub>3-*m*2</sub> somewhat agrees with that of 4.9 GPa obtained from experimental high pressure measurements.[(21)] The calculated transition pressure for the ZnSiO<sub>3-*m*1</sub> → ZnSiO<sub>3-*r*</sub> phase transition is 11.0 GPa and this agrees well with the experimental observation of pressure induced phase transition from ZnSiO<sub>3-*m*</sub> to -*r* at 10-12 GPa[(20-24)] and smaller than 15 GPa.[(26)] Furthermore, our studies of the pressure dependence of the volume for ZnSiO<sub>3-*r*</sub> (Fig. 5) is found to be in good agreement with recent experimental data from Ref.[(25)].

Bulk modulus ( $B_0$ ) is the parameter characterizing compressibility of a solid. Among the considered polymorphs of ZnSiO<sub>3</sub>, the calculated  $B_0$  values vary in the range from 47.4 GPa for ZnSiO<sub>3-*m*2</sub> to 235.8 GPa for ZnSiO<sub>3-*o*</sub> (Table I). These analysis shows that ZnSiO<sub>3-*o*</sub> is the hardest phase among the considered polymorphs. The pressure derivative of the bulk modulus ( $B_0'$ ) for some of the silicates is surprisingly large. It equals to 4.58 for ZnSiO<sub>3-*o*</sub>, 7.15 for ZnSiO<sub>3-*m*1</sub>, and 5.5 for ZnSiO<sub>3-*r*</sub>. We have cross checked the calculated bulk modulus and its pressure derivative with two independent fitting programs as well as with different equation of state models and arrived at the same results.

### 3.2 Zn<sub>2</sub>SiO<sub>4</sub>

From the structural optimization the equilibrium structural parameters for different polymorphs of Zn<sub>2</sub>SiO<sub>4</sub> have been calculated and presented in Table II. Analysis of the Table II shows that the calculated equilibrium volumes differ from the experimentally determined values by <1.4% for Zn<sub>2</sub>SiO<sub>4-*o*2</sub>, 3.2% for Zn<sub>2</sub>SiO<sub>4-*t*</sub> and 3.4% for Zn<sub>2</sub>SiO<sub>4-*r*</sub>. For Zn<sub>2</sub>SiO<sub>4-*m*</sub> the calculated equilibrium volume is considerable smaller by 8.6% from the experimentally determined one. The discrepancy between the calculated and experimental equilibrium volume for different polymorphs may be related to the difference in stoichiometry of the experimentally studied phases, temperature effects, and also uncertainty in some of the lattice and positional parameters. For example, the lattice parameters for Zn<sub>2</sub>SiO<sub>4-*m*</sub> and Zn<sub>2</sub>SiO<sub>4-*o*1</sub> in Ref. [(27)] correspond to non-stoichiometric crystals with atomic ratio of Zn:Si=1.7 and 1.9, respectively, whereas in our calculations the

atomic ratio was always Zn:Si=2. Overall the calculated positional parameters agree well with experimental data given in Table II. We have checked the symmetry of the lattices after structural relaxation and found that their symmetry remain the same as that of the experimentally determined one for all considered polymorphs.

Dependence of the total energy with volume for  $\text{Zn}_2\text{SiO}_4$ -*r*, -*t*, -*o*<sub>1</sub>, -*o*<sub>2</sub>, -*c*, -*o*<sub>3</sub> are displayed in Fig. 6. Among these polymorphs,  $\text{Zn}_2\text{SiO}_4$ -*r* possesses the largest equilibrium volume and smallest total energy at the minimum.  $\text{Zn}_2\text{SiO}_4$ -*c* posses the smallest equilibrium volume, but  $\text{Zn}_2\text{SiO}_4$ -*m* has largest total energy at  $E_{\text{tot}}^{\text{min}}$  among the considered phases. Consequently, according to our calculations  $\text{Zn}_2\text{SiO}_4$ -*r* is the most stable phase while  $\text{Zn}_2\text{SiO}_4$ -*m* is the least stable phase. In addition to the largest total energy, the dependence  $E_{\text{tot}}(V)$  for  $\text{Zn}_2\text{SiO}_4$ -*m* is crossed by that of  $\text{Zn}_2\text{SiO}_4$ -*o*<sub>1</sub> at its minimum. Consequently, even if  $\text{Zn}_2\text{SiO}_4$ -*m* has been formed, it can be transformed into  $\text{Zn}_2\text{SiO}_4$ -*o*<sub>1</sub>, without pressing or heating.

Analysis of Fig. 6 shows that the total energy variation with volume for  $\text{Zn}_2\text{SiO}_4$ -*r* intersects with  $\text{Zn}_2\text{SiO}_4$ -*t* at high pressure. At more volume compression,  $E_{\text{tot}}(V)$  for other polymorphs also intersect in the following sequence:  $\text{Zn}_2\text{SiO}_4$ -*t* with -*o*<sub>1</sub>, -*o*<sub>1</sub> with -*o*<sub>2</sub>, -*o*<sub>2</sub> with -*c*, and -*c* with -*o*<sub>3</sub>. This result indicates the possibility of pressure-induced phase transition, which is demonstrated in Fig. 7. The phase transition from  $\text{Zn}_2\text{SiO}_4$ -*r* to  $\text{Zn}_2\text{SiO}_4$ -*t* occurs at 0.8 GPa with volume shrinkage 7.3 Å<sup>3</sup>/f.u., whereas  $\text{Zn}_2\text{SiO}_4$ -*t* to  $\text{Zn}_2\text{SiO}_4$ -*o*<sub>1</sub> takes place at 15.0 GPa with very small volume shrinkage 0.8 Å<sup>3</sup>/f.u..  $\text{Zn}_2\text{SiO}_4$ -*o*<sub>1</sub> can exist at small pressure range and upon compression it can be transformed into  $\text{Zn}_2\text{SiO}_4$ -*o*<sub>2</sub>. The volume variation at the transition  $\text{Zn}_2\text{SiO}_4$ -*o*<sub>1</sub> to -*o*<sub>2</sub> occurring at 15.8 GPa, is ~4.7 Å<sup>3</sup>/f.u.. Upon compression  $\text{Zn}_2\text{SiO}_4$ -*o*<sub>2</sub> can transform into  $\text{Zn}_2\text{SiO}_4$ -*c* at 20.0 GPa (Fig. 7) with volume shrinkage 2.1 Å<sup>3</sup>/f.u.  $\text{Zn}_2\text{SiO}_4$ -*c* can be transformed to  $\text{Zn}_2\text{SiO}_4$ -*o*<sub>3</sub> at 24.9 GPa with small volume variation ~1.3 Å<sup>3</sup>/f.u. It should be noted that the present calculations are strictly speaking valid only for the stoichiometric compounds at low temperatures. In contrast off-stoichiometry and temperature could stabilize the experimentally identified high pressure polymorphs such as  $\text{Zn}_2\text{SiO}_4$ -*m*, -*o*<sub>1</sub>, -*o*<sub>2</sub>, and -*o*<sub>3</sub>. In order to clarify the origin of stability of these polymorphs at high pressures and low temperature high pressure experimental measurements on stoichiometric  $\text{Zn}_2\text{SiO}_4$  at low temperatures are needed.

The calculated bulk modulus for  $\text{Zn}_2\text{SiO}_4$  polymorphs (Table II) vary in the range from 63.0 GPa for  $\text{Zn}_2\text{SiO}_4$ -*m* to 235.8 GPa for  $\text{Zn}_2\text{SiO}_4$ -*o*<sub>3</sub>. It follows from these analyses that  $\text{Zn}_2\text{SiO}_4$ -*o*<sub>3</sub> is the hardly

compressible phase. The calculated bulk modulus and its pressure derivative for  $Zn_2SiO_4-c$  is found to be in good agreement (see Table II) with the respective experimentally determined values of 212 GPa and  $B_0' = 4$  for  $Mg_2SiO_4-c$ [(39)] and the bulk modulus of 216 GPa for  $Zn_2SiO_4-c$ [(23)]. This result indicates that the valence and bonding behavior of  $Zn_2SiO_4$  is similar to that of the geochemically important material  $Mg_2SiO_4$ . However, among the considered  $Zn_2SiO_4$  polymorphs,  $Zn_2SiO_4-m$  is found to be the softest phase.

#### 4. Discussion

One of the important questions is which of the  $ZnSiO_3$  and  $Zn_2SiO_4$  polymorphs can be formed at the interface  $ZnO-Si(SiO_2)$  and how it depends on growth and device operation conditions. Although some preliminary studies are already available in literature, there is no systematic study of the point. For example, a crystalline  $ZnSiO_3$  is formed[(40)] upon irradiation of nanocomposite  $ZnO-SiO_2$  films with ultraviolet light because of the photo-induced reaction. From analysis of secondary ion mass spectroscopy inter-diffusion of  $Zn(Si)$  into  $Si(ZnO)$  has been reported at the interface between  $ZnO$  film and  $Si$  substrate.[(2)] By means of cathodoluminescence and glancing-angle X-ray diffraction the tetragonal modification of  $Zn_2SiO_4$  was proved to be present.  $Zn_2SiO_4$  is also formed at the interface of  $ZnO/Si$  heterostructures.[(5, 2, 41)] It can form large band offset with  $Si$  and  $ZnO$ ,[(5)] which is assumed to be one of the reasons for low 8.5 % efficiency of crystalline  $Si-ZnO$  solar cells.[(3)] Formation of rhombohedral modification of  $Zn_2SiO_4$  at the boundary between  $ZnO$  particles and  $SiO_2$  matrix has also been reported.[(16)] These findings are important and indicate that the idea about formation of the zinc silicates is not far from reality. From the theoretical study of the present paper we found that  $ZnSiO_3-m_1$  and  $Zn_2SiO_4-r$  are the most stable polymorphs. Systematic experimental study of this point is needed.

The other important point is the pressure at which the stable polymorphs  $ZnSiO_3-m_1$  and  $Zn_2SiO_4-r$  can be transformed into another one. Analysis of the above theoretical findings corresponding to  $T=0$  K and experimental results corresponding to high temperatures indicate that the transition pressure is very large, which might not be available in  $ZnSiO_3$  or  $Zn_2SiO_4$  containing device structures. Consequently, possibility of phase transitions at ambient pressures ( $<6.82$  GPa for  $ZnSiO_3$  and  $<0.80$  GPa for  $Zn_2SiO_4$ ) can be excluded. This

finding has important implications such as, for example, the possibility of lattice expansion/shrinkage, phase-transition-induced abnormal temperature dependence of electrical conductivities experimentally observed[(42)] in ZnTe:Cu can also be excluded.

Comparative analysis[(32)] of electronic structure and optical properties of the ZnSiO<sub>3</sub> and Zn<sub>2</sub>SiO<sub>4</sub> shows that optical parameters and conduction band electron effective masses of the compounds are almost isotropic and their dependence on crystal structure is negligible. Furthermore, the calculated absorption coefficient, reflectivity, refractive index, and extinction coefficients are  $<10^3 \text{ cm}^{-1}$ , 0.15, 2.2, and 0.3, respectively, which indicate the possibility of using the zinc silicates as antireflection coatings. Consequently, pressure-induced phase transitions is not expected to cause modulation of optical properties of the ZnO-ZnSiO<sub>3</sub>(Zn<sub>2</sub>SiO<sub>4</sub>)-Si based device structures.

## 5. Conclusion

Phase stability and pressure-induced structural transition between different polymorphs of ZnSiO<sub>3</sub> and Zn<sub>2</sub>SiO<sub>4</sub> have been studied based on *ab initio* total energy calculations. Among the monoclinic phase with space groups  $P2_1/c$  and  $C2/c$ , rhombohedral ( $\bar{R}3$ ), and orthorhombic ( $Pbca$ ) modifications, the low pressure monoclinic ZnSiO<sub>3</sub> phase is found to be the most stable one. Two sequences of structural phase transitions between different modifications of the ZnSiO<sub>3</sub> have been found. One sequence is from ZnSiO<sub>3</sub> ( $P2_1/c$ ) to ZnSiO<sub>3</sub>-( $C2/c$ ) and the other one is from ZnSiO<sub>3</sub>-( $C2/c$ ) to ZnSiO<sub>3</sub>- $\bar{R}3$ . At high pressure monoclinic ZnSiO<sub>3</sub> ( $C2/c$ ) can coexist with orthorhombic ( $Pbca$ ) and equilibrium volume and total energy corresponding to these two polymorphs are found to be slightly different from each other. This indicates that small fluctuation in environment can be sufficient for orthorhombic to monoclinic transition, which could also explain why the orthorhombic phase is metastable under all conditions. These two polymorphs are found to co-exist in a certain pressure and volume range. According to present total energy calculations ilmenite form of ZnSiO<sub>3</sub> is found to be the most unstable one at low temperatures and high pressures. Distinct from previous experimental studies at high temperatures, no pressure-induced phase transition has been found into/from this modification. This

indicates that the ilmenite phase of  $\text{ZnSiO}_3$  may be stabilized by the lattice dynamics or oxygen stoichiometry. Among the rhombohedral, tetragonal, orthorhombic, orthorhombic, cubic, and orthorhombic modifications of  $\text{Zn}_2\text{SiO}_4$  rhombohedral phase is found to be most stable. It can be transformed into tetragonal phase at high pressures, which upon further compression transformed into spinel modification. The calculated transition pressures agree with experimental data. Based on analogy with  $\text{Mg}_2\text{SiO}_4$  orthorhombic  $\text{Zn}_2\text{SiO}_4$  has been studied. It is found that this polymorph possesses relatively large bulk modulus and, consequently, can be considered as hardly compressible phase. The presently considered silicates can exist at the interface between  $\text{ZnO}$  and  $\text{Si}(\text{SiO}_2)$ . Although the reported structural transformation between the zinc silicate polymorphs is possible, the transitions occur at high pressures. So, at low pressures, the phase transition-induced lattice expansion/shrinkage or modulation of the electronic structure and optical properties of the device structures with  $\text{ZnSiO}_3$  and  $\text{Zn}_2\text{SiO}_4$  is not expected.

### **Acknowledgments**

This work has received financial and supercomputing support from the Research Council of Norway within FUNMAT and NANOMAT projects, as well as from the Academy of Sciences of Uzbekistan. SZK thanks A. Klaveness for useful discussions and computational help.

## References

1. He HP, Wang YX, Zou YM. 2003 Dec 7 Photoluminescence property of ZnO-SiO<sub>2</sub> composites synthesized by sol-gel method. *J Phys D: Appl Phys* **36**(23), 2972-5.
2. Xu X, Wang P, Qi Z, Hai M, Xu J, Liu H, et al. 2003 Formation mechanism of Zn<sub>2</sub>SiO<sub>4</sub> crystal and amorphous SiO<sub>2</sub> in ZnO/Si system. *J Phys: Condens Matter* **15**(40), L607-L13.
3. Kluth O, Rech B, Houben L, Wieder S, Schope G, Beneking C, et al. 1999 Aug 30 Texture etched ZnO : Al coated glass substrates for silicon based thin film solar cells. *Thin Solid Films* **351**(1-2), 247-53.
4. Kobayashi H, Mori H, Ishida T, Nakato Y. 1995 Feb 1 Zinc-Oxide N-Si Junction Solar-Cells Produced by Spray-Pyrolysis Method. *J Appl Phys* **77**(3), 1301-7.
5. Meier U, Pettenkofer C. 2005 Nov 15 Morphology of the Si-ZnO interface. *Appl Surf Sci* **252**(4), 1139-46.
6. Xu XL, Wang P, Qi ZM, Ming H, Xu J, Liu HT, et al. 2003 Oct 15 Formation mechanism of Zn<sub>2</sub>SiO<sub>4</sub> crystal and amorphous SiO<sub>2</sub> in ZnO/Si system. *J Phys: Condens Matter* **15**(40), L607-L13.
7. Birkmire RW. 2001 2001/1 Compound polycrystalline solar cells:: Recent progress and Y2 K perspective. *Sol Energy Mater Sol Cells* **65**(1-4), 17-28.
8. Nakanishi Y, Miyake A, Tatsuoka H, Kominami H, Kuwabara H, Hatanaka Y. 2005 May 15 HRTEM observation of interface states between ZnO epitaxial film and Si(111) substrate. *Appl Surf Sci* **244**(1-4), 359-64.
9. Chen H, Zhong J, Saraf G, Lu Y, Hill DH, Hsu ST, et al. 2006 Jun Interface properties of ZnO nanotips grown on Si substrates. *J Electron Mater* **35**(6), 1241-5.
10. Amekura H, Kono K, Kishimoto N, Buchal C. 2006 Jan Formation of zinc-oxide nanoparticles in SiO<sub>2</sub> by ion implantation combined with thermal oxidation. *Nucl Instrum Methods Phys Res, Sect B* **242**(1-2), 96-9.
11. Amekura H, Sakuma Y, Kono K, Takeda Y, Kishimoto N, Buchal C. 2006 Apr 1 Luminescence from ZnO nanoparticles/SiO<sub>2</sub> fabricated by ion implantation and thermal oxidation. *Phys B-Condens Matter* **376**, 760-3.

12. Amekura H, Umeda N, Sakuma Y, Plaksin OA, Takeda Y, Kishimoto N, et al. 2006 Apr 10 Zn and ZnO nanoparticles fabricated by ion implantation combined with thermal oxidation, and the defect-free luminescence. *Appl Phys Lett* **88**(15).
13. Amekura H, Umeda N, Yoshitake M, Kono K, Kishimoto N, Buchal C. 2006 Jan 18 Formation processes of zinc-oxide nanoparticles by ion implantation combined with thermal oxidation. *J Cryst Growth* **287**(1), 2-6.
14. Cai Y, Sandhage KH. 2005 Aug Zn<sub>2</sub>SiO<sub>4</sub>-coated microparticles with biologically-controlled 3D shapes. *Phys Stat Solidi A* **202**(10), R105-R7.
15. Emel'chenko GA, Gruzintsev AN, Koval'chuk MN, Masalov VM, Samarov EN, Yakimov EE, et al. 2005 Opal-ZnO nanocomposites: Structure and emission properties. *Semicond* **39**(11), 1328-32.
16. Ma JG, Liu YC, Xu CS, Liu YX, Shao CL, Xu HY, et al. 2005 May 15 Preparation and characterization of ZnO particles embedded in SiO<sub>2</sub> matrix by reactive magnetron sputtering. *J Appl Phys* **97**(10).
17. Yuk JM, Lee JY, No YS, Kim TW, Choi WK. 2008 Dec 1 Transformation mechanisms from metallic Zn nanocrystals to insulating ZnSiO<sub>3</sub> nanocrystals in a SiO<sub>2</sub> matrix due to thermal treatment. *Appl Phys Lett* **93**(22), 221910.
18. Shin JW, No YS, Kim TW, Choi WK. 2008 Oct Formation and Microstructural Properties of Locally Distributed ZnSiO<sub>3</sub> Nanoparticles Embedded in a SiO<sub>2</sub> Layer by Using a Focused Electron Beam. *J Nanosci Nanotechnol* **8**(10), 5566-70.
19. Yuk JM, Lee JY, Jung JH, Lee DU, Kim TW, Son DI, et al. 2008 Apr 15 Formation mechanism of ZnSiO<sub>3</sub> nanoparticles embedded in an amorphous interfacial layer between a ZnO thin film and an n-Si (001) substrate due to thermal treatment. *J Appl Phys* **103**(8), 083520.
20. Akaogi M, Yusa H, Ito E, Yagi T, Suito K, Iiyama JT. 1990 The ZnSiO<sub>3</sub> Clinopyroxene-Ilmenite Transition - Heat-Capacity, Enthalpy of Transition, and Phase-Equilibria. *Phys Chem Miner* **17**(1), 17-23.
21. Arlt TT, Angel RJ. 2000 Displacive phase transitions in C-centred clinopyroxenes: spodumene, LiScSi<sub>2</sub>O<sub>6</sub> and ZnSiO<sub>3</sub>. *Phys Chem Miner* **27**(10), 719-31.

22. Ito E, Matsui Y. 1979 High-Pressure Transformations in Silicates, Germanates, and Titanates with  $Abo_3$  Stoichiometry. *Phys Chem Miner* **4**(3), 265-73.
23. Leinenweber K, Navrotsky A, McMillan P, Ito E. 1989 Transition Enthalpies and Entropies of High-Pressure Zinc Metasilicates and Zinc Metagermanates. *Phys Chem Miner* **16**(8), 799-808.
24. Morimoto N, Nakajima Y, Syono Y, Akimoto S, Matsui Y. 1975 Crystal-Structures of Pyroxene-Type  $ZnSiO_3$  and  $ZnMgSi_2O_6$ . *Acta Crystallogr, Sect B: Struct Sci* **B 31**(APR15), 1041-9.
25. Sato Y, Ito E, Akimoto SI. 1977 Hydrostatic Compression of Ilmenite Phase of  $ZnSiO_3$  and  $MgGeO_3$ . *Phys Chem Miner* **2**(1-2), 171-6.
26. Ito E, Matsui Y. 1975 High-Pressure Synthesis of  $ZnSiO_3$  Ilmenite. *Phys Earth Planet Interiors* **9**(4), 344-52.
27. Syono Y, Akimoto SI, Matsui Y. 1971 High Pressure Transformations in Zinc Silicates. *J Solid State Chem* **3**(3), 369-80.
28. Kim HW, Shim SH, Lee JW, Lee C, Jeoung SC. 2008 Mar ZnO-sheathed SiOx nanowires: Annealing effect. *Opt Mater* **30**(7), 1221-4.
29. Chen JK, Tang KL, Tang TP, Chang JT. 2008 Jul Effects of zinc oxide and porosity on permittivity of sintered zinc sulfide-silicon dioxide. *Jpn J Appl Phys* **47**(7), 5539-44.
30. Cheng BC, Yu XM, Liu HJ, Wang ZG. 2008 Oct  $Zn_2SiO_4/ZnO$  Core/Shell Coaxial Heterostructure Nanobelts Formed by an Epitaxial Growth. *J Phys Chem C* **112**(42), 16312-7.
31. Marumo F, Syono Y. 1971 Crystal Structure of  $Zn_2SiO_4$ -II, a High-Pressure Phase of Willemite. *Acta Crystallogr, Sect B: Struct Cryst* **B 27**(OCT15), 1868.
32. Karazhanov SZ, Ravindran P, Fjellvag H, Svensson BG. 2009 Electronic structure and optical properties of  $ZnSiO_3$  and  $Zn_2SiO_4$ . *Phys Rev B* **Submitted**.
33. Blochl PE. 1994 Projector augmented-wave method. *Phys Rev B* **50**(24), 17953-79.
34. Kresse G, Joubert D. 1999 *Phys Rev B* **59**, 1758.
35. Kresse G, Furthmüller J. 1996 Efficient iterative schemes for ab initio total-energy calculations using a plane-wave basis set. *Phys Rev B* **54**(16), 11169-86.

36. Ceperley DM, Alder BJ. 1980 *Phys Rev Lett* **45**, 566.
37. Perdew JP, Zunger A. 1981 *Phys Rev B* **23**, 5048.
38. Inorganic Crystal Structure Database. Karlsruhe: Gmelin Institut; 2001.
39. Ito E, Akaogi M, Topor L, Navrotsky A. 1990 Sep 14 Negative Pressure-Temperature Slopes for Reactions Forming MgSiO<sub>3</sub> Perovskite from Calorimetry. *Science* **249**(4974), 1275-8.
40. Taghavinia N, Lee HY, Makino H, Yao T. 2005 Jun Evolution of roughness and photo-crystallization effect in ZnS-SiO<sub>2</sub> nanocomposite films. *Nanotechnol* **16**(6), 944-8.
41. Xu XL, Guo CX, Qi ZM, Liu HT, Xu J, Shi CS, et al. 2002 Sep 23 Annealing effect for surface morphology and luminescence of ZnO film on silicon. *Chem Phys Lett* **364**(1-2), 57-63.
42. Zhang J-q, Feng L-h, Cai W, Zheng J-g, Cai Y-p, Li B, et al. 2002 2002/7/1 The structural phase transition and mechanism of abnormal temperature dependence of conductivity in ZnTe:Cu polycrystalline thin films. *Thin Solid Films* [doi: DOI: 10.1016/S0040-6090(02)00451-0] **414**(1), 113-8.
43. Simonov MA, Sandomirskii PA, Egorovtismenko IK, Belov NV. 1977 Crystal-Structure of Willemite, Zn<sub>2</sub>SiO<sub>4</sub>. *Dokl Akad Nauk SSSR* **237**(3), 581-4.

Table I Unit-cell dimensions and volumes, positional parameters, bulk modulus ( $B_0$ ), as well as the derivative of bulk modulus ( $B_0'$ ) for  $\text{ZnSiO}_3$ ,  $-o$ ,  $-m_1$ ,  $-m_2$ ,  $-m_3$ ,  $-m_4$ ,  $-r_1$ , and  $-r_2$  derived from the density functional total energy calculations at the total energy minimum. Values given in parentheses refer to experimental data. [(38)] The unit cell volumes are presented per formula unit in  $\text{\AA}^3$ .

Compound	Unit cell ( $\text{\AA}$ )	Atom	Site	X	Y	Z	$B_0$ (GPa)	$B_0'$
$\text{ZnSiO}_3$ - $o$	$a=17.4224(18.2040)^a$	Zn1	$8c$	0.1253 (0.1255)	0.3557 (0.3559)	0.4007 (0.4039)	235.8	4.58
$Pbca$	$b=8.7544(9.0870)^a$	Zn2	$8c$	0.3760 (0.3761)	0.5140 (0.5092)	0.3949 (0.4005)		
	$c=5.0881(5.2780)^a$	Si1	$8c$	0.2742 (0.2741)	0.3373 (0.3363)	0.0852 (0.0867)		
	$V=53.32(54.57)^a$	Si2	$8c$	0.4717 (0.4730)	0.1677 (0.1656)	0.2872 (0.2839)		
		O1	$8c$	0.1840 (0.1853)	0.3318 (0.3346)	0.0831 (0.0820)		
		O2	$8c$	0.3108 (0.3115)	0.4995 (0.4966)	0.1045 (0.1040)		
		O3	$8c$	0.3032 (0.3039)	0.2503 (0.2521)	0.3368 (0.3400)		
		O4	$8c$	0.5624 (0.5621)	0.3355 (0.3389)	0.7863 (0.7800)		
		O5	$8c$	0.4301 (0.4327)	0.4811 (0.4853)	0.6999 (0.7040)		
		O6	$8c$	0.4473 (0.4488)	0.2049 (0.2100)	0.5805 (0.5710)		
$\text{ZnSiO}_3$ - $m_1$	$a=9.6543(9.5781)^b$	Zn1	$4e$	0.2494 (0.2508)	0.6465 (0.6509)	0.2332 (0.2247)	66.5	7.15
$P2_1/c$	$b=9.0667(8.8905)^b$	Zn2	$4e$	0.2530 (0.2551)	0.0129 (0.0034)	0.2312 (0.2211)		
	$c=5.2653(5.1798)^b$	Si1	$4e$	0.0507 (0.0468)	0.3370 (0.3403)	0.2906 (0.2924)		
	$V=53.69(51.99)^b$	Si2	$4e$	0.5583 (0.5568)	0.8332 (0.8338)	0.2500 (0.2397)		
	$\beta=111.26(109.443)^b$	O1	$4e$	0.8693 (0.8691)	0.3323 (0.3386)	0.1652 (0.1800)		
		O2	$4e$	0.3764 (0.3779)	0.8362 (0.8367)	0.1309 (0.1300)		
		O3	$4e$	0.1231 (0.1169)	0.5000 (0.5033)	0.3537 (0.3365)		
		O4	$4e$	0.6382 (0.6341)	0.9845 (0.9828)	0.3906 (0.3895)		
		O5	$4e$	0.1119 (0.1090)	0.2529 (0.2662)	0.5850 (0.5982)		
		O6	$4e$	0.6079 (0.6078)	0.7051 (0.6965)	0.4893 (0.4702)		
$\text{ZnSiO}_3$ - $m_2$	$a=9.3173(9.787)^a$	Zn1	$4e$	0.5000 (0.5000)	0.3921 (0.3919)	0.2500 (0.2500)	47.4	4.2
$C2/c$	$b=9.8180(9.161)^a$	Zn2	$4e$	0.5000 (0.0000)	0.7289 (0.2361)	0.2500 (0.2500)	(72.0) <sup>b</sup>	(7.0) <sup>b</sup>
	$c=5.0898(5.296)^a$	Si1	$8f$	0.3060 (0.3016)	0.0837 (0.0849)	0.2646 (0.2668)	(101.0)	
	$V=53.92(55.26)^a$	O1	$8f$	0.1238 (0.1241)	0.0833 (0.0868)	0.1427 (0.1473)		
	$\beta=111.80(111.42)^a$	O2	$8f$	0.3839 (0.3787)	0.2390 (0.2393)	0.3783 (0.3719)		
		O3	$8f$	0.3583 (0.3533)	0.0321 (0.0238)	0.0184 (0.0273)		
$\text{ZnSiO}_3$ - $r$	$a=4.8115(4.7469)^c$	Zn	$6c$	0.0000 (0.0000)	0.0000 (0.0000)	0.3692 (0.3599)	177.89	5.5
$R\bar{3}$	$c=13.9974(13.754)^c$	Si	$6c$	0.0000 (0.0000)	0.0000 (0.0000)	0.1607 (0.1556)	(216.0) <sup>c,d</sup>	
	$V=46.77(44.73)^c$	O	$18f$	0.9911 (0.9645)	0.3736 (0.3200)	0.4286 (0.4896)		

<sup>a</sup>From Ref. [(38)].

<sup>b</sup>From Ref. [(21)].

<sup>c</sup>From Ref. [(23)].

<sup>d</sup>From Ref. [(23, 25)].

Table II Unit-cell dimensions, equilibrium volumes, positional parameters, bulk modulus ( $B_0$ ), and the pressure derivative of bulk modulus ( $B_0'$ ) for  $Zn_2SiO_4$   $-t$ ,  $-r$ ,  $-m$ ,  $-o_1$ ,  $-o_2$ , and  $-c$  derived from the density functional total energy calculations at the total energy minimum. Values given in parentheses refer to experimental data. [(38)]

Compound	Unit cell (Å)	Atom	Site	X	Y	Z	$B_0$ (GPa)	$B_0'$
$Zn_2SiO_4-r$	$a=13.8469(13.971)^a$	Zn1	$18f$	0.1908 (0.1916)	0.2098 (0.2087)	0.5843 (0.5844)	138.8	3.3
$R\bar{3}$	$c=9.1781(9.3340)^a$	Zn2	$18f$	0.5264 (0.5579)	0.8818 (0.9655)	0.5841 (0.5815)		
	$V=84.670(87.66)^a$	Si	$18f$	0.1951 (0.1963)	0.2127 (0.2118)	0.2499 (0.2510)		
		O1	$18f$	0.7924 (0.8767)	0.5435 (0.5415)	0.4376 (0.3918)		
		O2	$18f$	0.1271 (0.1295)	0.2063 (0.3178)	0.3974 (0.3955)		
		O3	$18f$	0.1083 (0.1100)	0.2127 (0.2175)	0.7507 (0.7496)		
		O4	$18f$	0.9854 (0.9335)	0.6568 (0.6283)	0.5838 (0.5007)		
$Zn_2SiO_4-t$	$a=6.9562(7.0069)^b$	Zn	$8d$	0.1549 (0.1570)	0.2500 (0.2500)	0.1250 (0.1250)	135.8	1.3
$I\bar{4}2d$	$c=6.3533(6.4637)^b$	Si	$4b$	0.0000 (0.0000)	0.0000 (0.0000)	0.5000 (0.5000)		
	$V=76.86(79.38)^b$	O	$16e$	0.3054 (0.3079)	0.4832 (0.4890)	0.1070 (0.1376)		
$Zn_2SiO_4-m$	$a=5.3752(5.069)^c$	Zn1	$4e$	0.3542	0.3811	0.5969	63.0	1.7
$P2_1/n$	$b=7.8794(10.292)^c$	Zn2	$4e$	0.4476	0.9915	0.3091		
	$c=7.5624(6.667)^c$	Si	$4e$	0.1760	0.7380	0.5414		
	$V=79.55(87.0)^c$	O1	$4e$	0.2697	0.9276	0.5053		
	$\beta=96.55(\sim 90)^c$	O2	$4e$	0.0135	0.7350	0.7089		
		O3	$4e$	0.4237	0.6246	0.5874		
		O4	$4e$	0.0019	0.6468	0.3805		
$Zn_2SiO_4-o_1$	$a=4.7231(4.79)^c$	Zn1	$4a$	0.0000	0.0000	0.0000	157.8	4.3
$Pbnm$	$b=10.1975(10.3)^c$	Zn2	$4c$	0.9850	0.2803	0.2500		
	$c=5.9430(6.02)^c$	Si	$4c$	0.4259	0.0960	0.2500		
	$V=71.56(74.25)^c$	O1	$4c$	0.7642	0.0936	0.2500		
		O2	$4c$	0.2164	0.4491	0.2500		
		O3	$8d$	0.2797	0.1643	0.0335		
$Zn_2SiO_4-o_2$	$a=5.8096(5.740)^c$	Zn1	$4a$	0.0000	0.0000	0.0000	222.0	11.1
$Imma$	$b=11.6392(11.504)^c$	Zn2	$4e$	0.2500	0.7500	0.4683		
	$c=8.5397(8.395)^c$	Zn3	$8g$	0.2500	0.1254	0.2500		
	$V=69.29(69.30)^c$	Si	$8h$	0.0000	0.1208	0.6164		
		O1	$4e$	0.0000	0.2500	0.2125		
		O2	$4e$	0.0000	0.2500	0.7130		
		O3	$8h$	0.0000	0.4873	0.7579		
		O4	$16j$	0.2639	0.1229	0.9917		
$Zn_2SiO_4-o_3$	$a=4.8891$	Zn	$8c$	0.9964	0.0553	0.3367	235.8	4.6
$Pbca$	$b=4.9980$	Si	$4a$	0.0000	0.0000	0.0000		
	$c=10.1666$	O1	$8c$	0.2012	0.2874	0.0494		
	$V=62.11$	O2	$8c$	0.8850	0.9553	0.1588		
$Zn_2SiO_4-c$	$a=8.0755^c$	Zn	$8b$	0.5000	0.5000	0.5000	222.2	4.6
$Fd\bar{3}m$	$V=65.83^c$	Si	$32e$	0.8750	0.8750	0.8750		
		O	$32e$	0.2438	0.2438	0.2438		

<sup>a</sup> From Ref. [(43)].

<sup>b</sup> From Ref. [(31)].

<sup>c</sup> Only lattice parameters of Ref. [(27)]. have been used and the positional parameters are from Ref. [(38)] with similar chemical formula and SG, i.e.  $Ca_2SiO_4$  type structure with SG  $P2_1/n$  for  $Zn_2SiO_4-m$ ,  $Ca_2RuO_4$  type structure with SG  $Pbca$  for  $Zn_2SiO_4-o_3$ ,  $Mg_2SiO_4$  type structure with SG  $Imma$  for  $Zn_2SiO_4-o_2$ ,  $Mg_2SiO_4$  type structure with SG  $Pbnm$  for  $Zn_2SiO_4-o_1$  have been used for the present computations. Lattice and positional parameters for  $Zn_2SiO_4-c$  we have used  $Mg_2SiO_4$  type structure with SG  $Fd\bar{3}m$ .

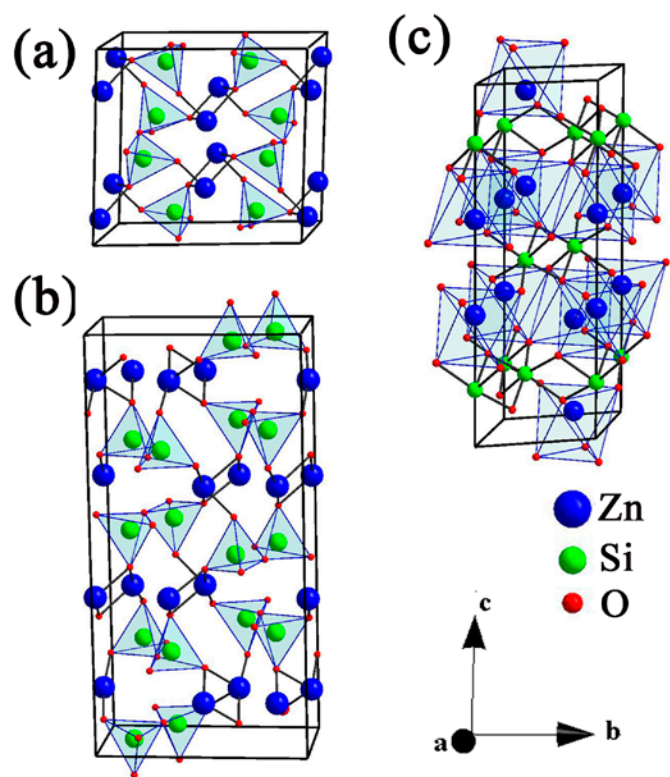


Fig. 1. Crystal structures of (a) ZnSiO<sub>3-m2</sub>, (b) ZnSiO<sub>3-o</sub>, and (c) ZnSiO<sub>3-r</sub>.

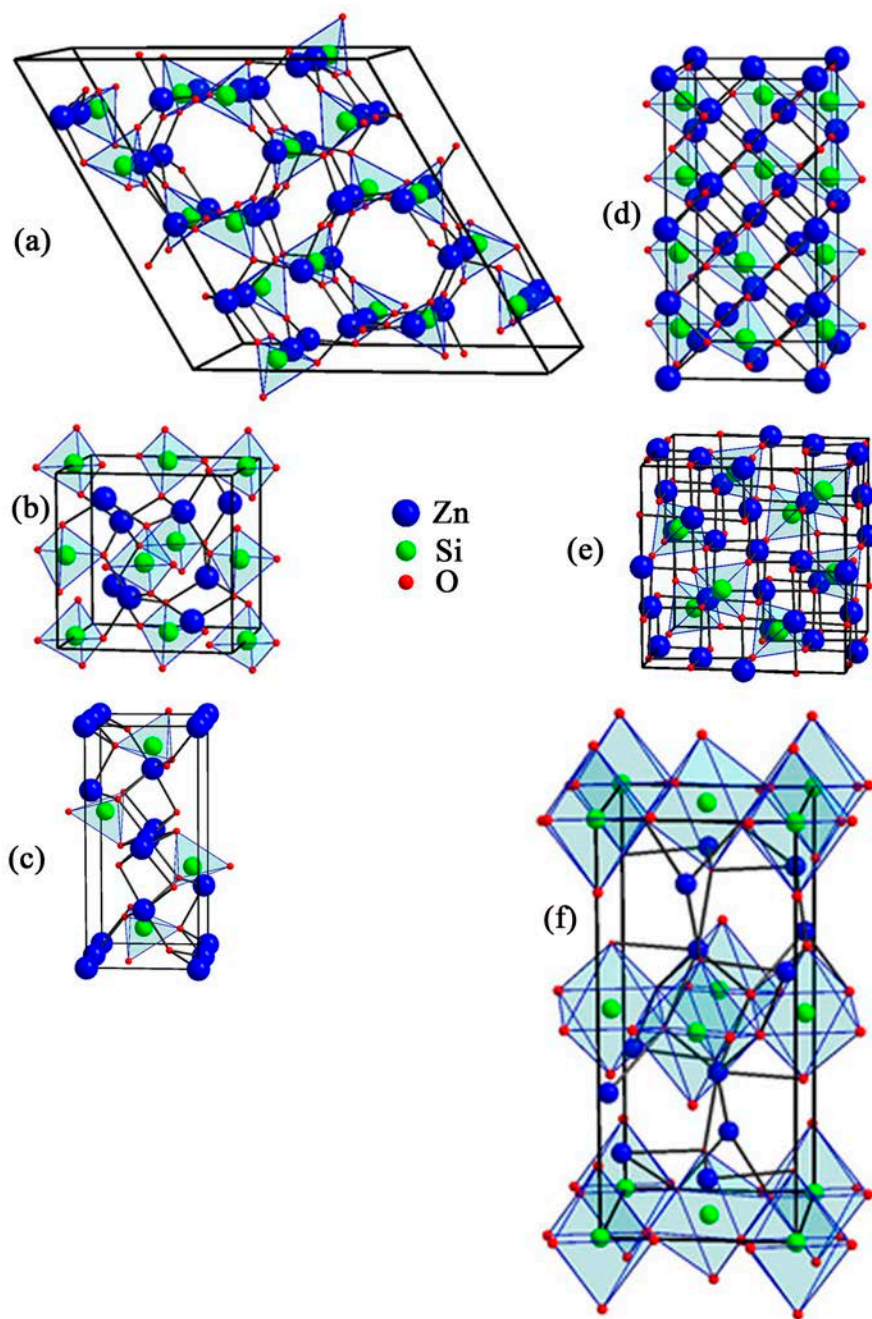


Fig. 2. Crystal structures of (a)  $Zn_2SiO_4-r$ , (b)  $Zn_2SiO_4-t$ , (c)  $Zn_2SiO_4-o_1$ , (d)  $Zn_2SiO_4-o_2$ , (e)  $Zn_2SiO_4-c$ , (f)  $Zn_2SiO_4-o_3$ .

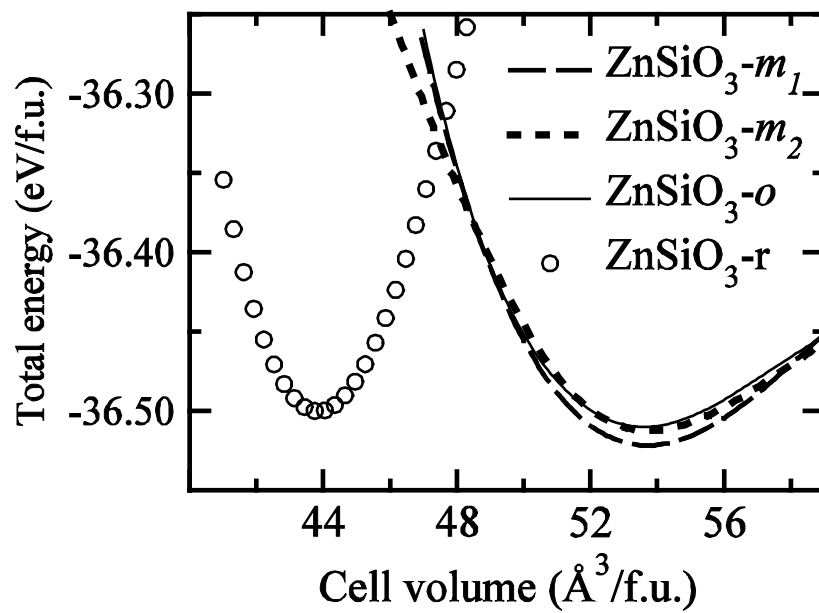


Fig. 3. Total energy vs volume curves for  $\text{ZnSiO}_3\text{-}m_1$ ,  $\text{-}m_2$ ,  $\text{-}o$ , and  $\text{-}r$ .

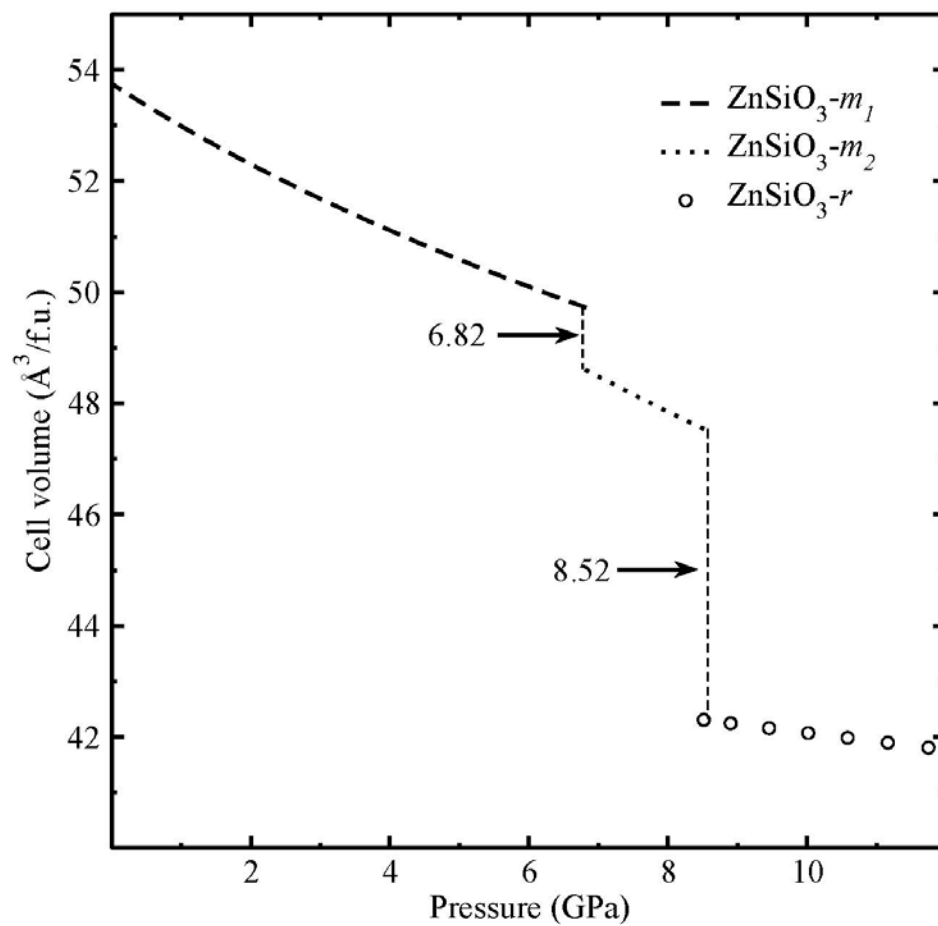


Fig. 4. Calculated cell volume vs pressure for  $\text{ZnSiO}_3\text{-}m_1$ ,  $\text{-}m_2$ , and  $\text{-}r$ .

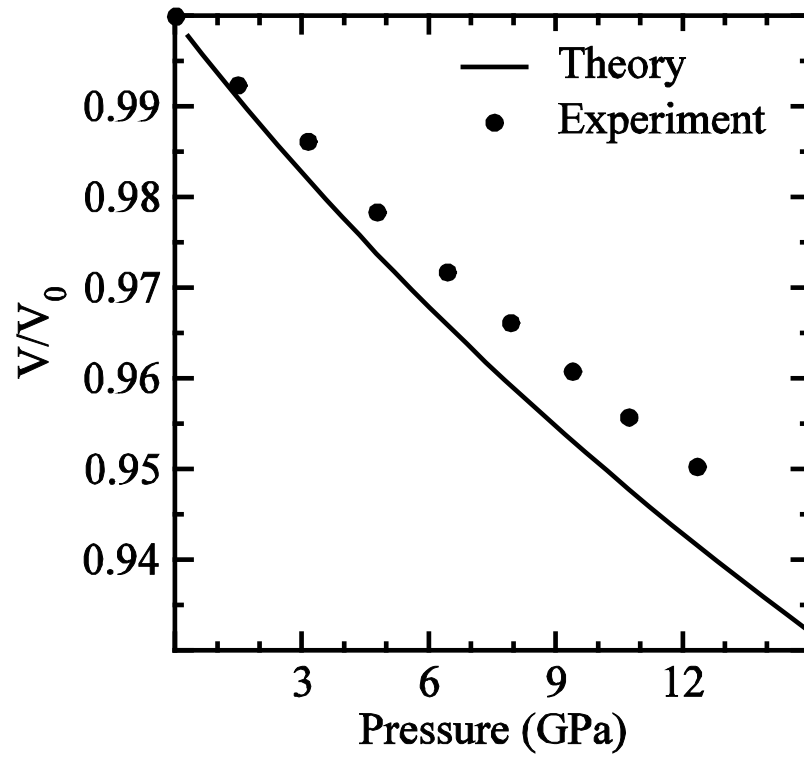


Fig. 5. Pressure dependence of the cell volume for  $\text{ZnSiO}_{3-r}$  along with the available experimental data from Ref. [(25)]

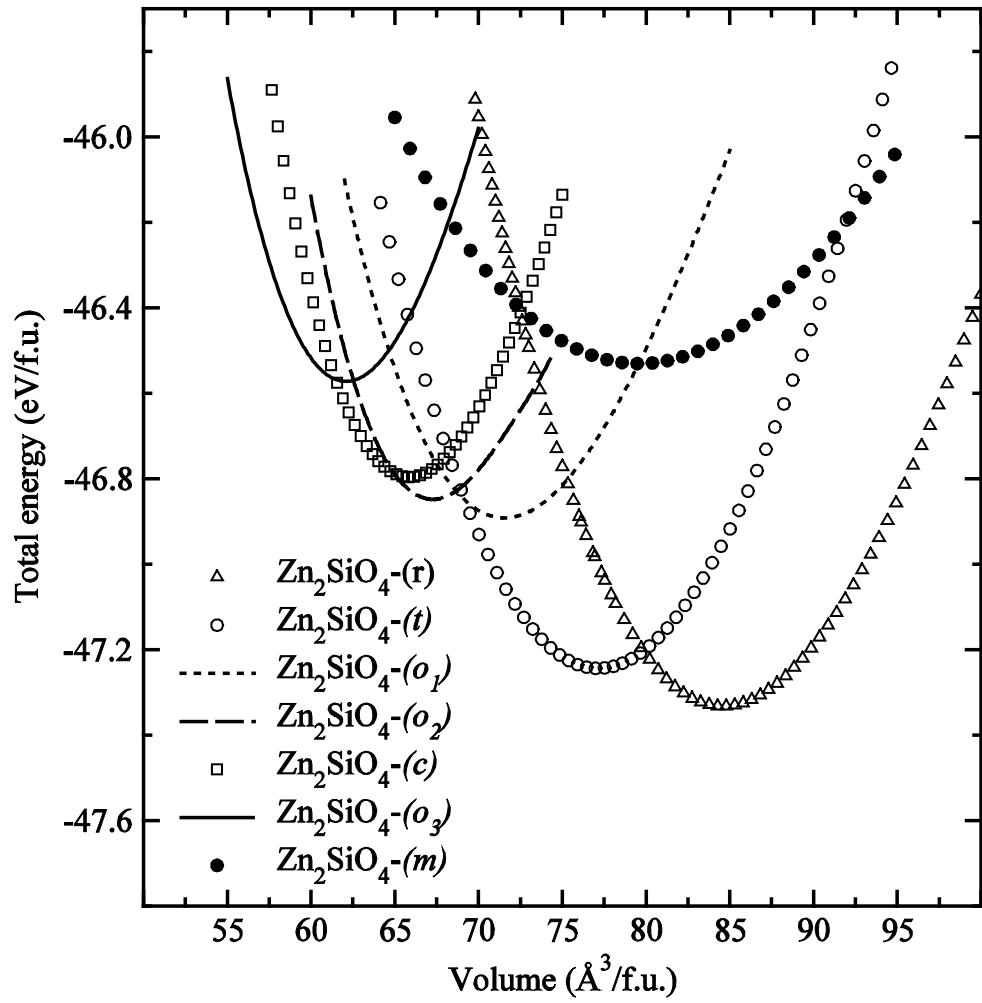


Fig. 6. Total energy vs volume for  $\text{Zn}_2\text{SiO}_4\text{-}r$ ,  $-t$ ,  $-o_1$ ,  $-o_2$ ,  $-c$ ,  $-o_3$ , and  $-m$ .

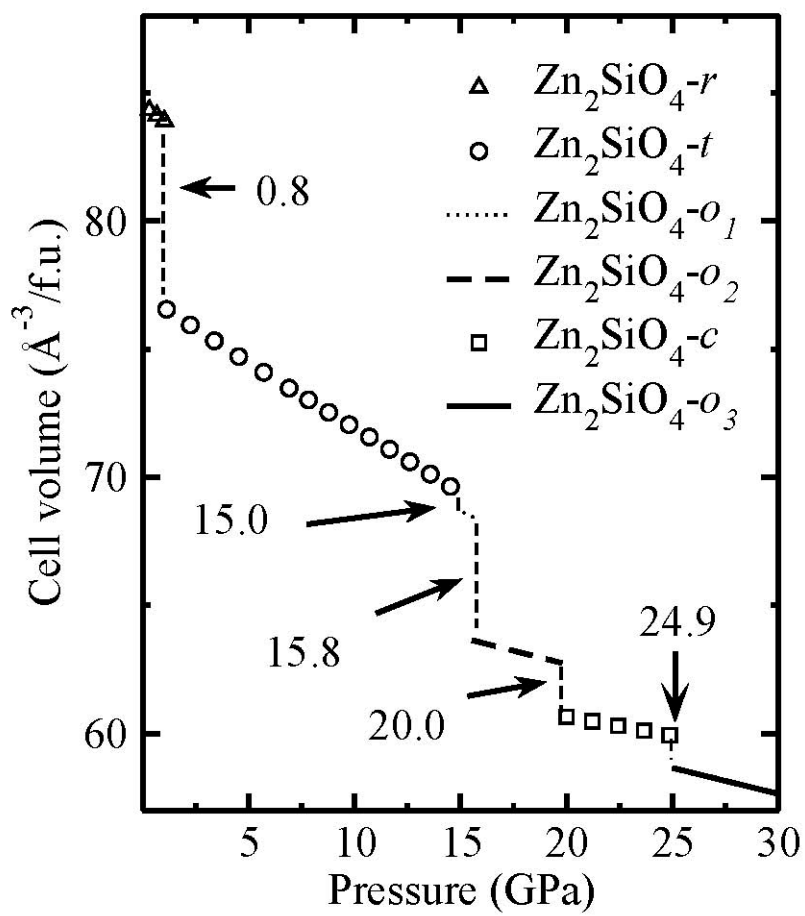


Fig. 7. Calculated cell volume vs pressure for  $\text{Zn}_2\text{SiO}_4\text{-}r$ ,  $\text{-}t$ ,  $\text{-}o_1$ ,  $\text{-}o_2$ ,  $\text{-}c$ , and  $\text{-}o_3$ .